machines

MDPI

Article

Research on Optimization Parameter Selection Method for Hull Form Optimization

Qiang Zheng [1,2], Baiwei Feng [1,2,*], Zuyuan Liu [1,2], Chengsheng Zhan [1,2] and Xide Cheng [1,2]

[1] Key Laboratory of High Performance Ship Technology, Ministry of Education, Wuhan 430063, China; zq451535308@163.com (Q.Z.)
[2] School of Shipbuilding, Marine Engineering, Energy and Power Engineering, Wuhan University of Technology, Wuhan 430063, China
* Correspondence: fengbaiwei@126.com

Abstract

Hull form optimization is a key technical approach for developing energy-efficient ship hulls. However, selecting appropriate optimization parameters remains challenging. Traditional methods often rely heavily on designer experience, leading to subjective and inconsistent parameter choices. Consequently, optimization results vary significantly and lack generalizability. This study focuses on container ships, using the KCS model to investigate the impact of optimization parameter distribution and hull surface deformation on wave-making resistance. Through systematic analysis, an optimized parameter selection methodology is developed, resulting in significant improvements in wave-making resistance performance for container ships. Specifically, a 20.28% reduction in wave-making resistance and a −3.01% reduction in total resistance are achieved.

Keywords: parameter selection; hull form optimization; surface deformation; container ship; wave-making resistance

1. Introduction

Maritime trade plays a vital role in global commerce. As the primary carriers for maritime trade, ships have garnered significant attention worldwide. Various energy-saving technologies exist for ships, among which hull form optimization based on Computational Fluid Dynamics (CFD) is a major research focus internationally. The recent International Towing Tank Conference (ITTC) highlighted Simulation-Based Design (SBD) as a key topic in numerical simulation technology research.

The SBD-based hull form optimization framework is illustrated in Figure 1. The process involves an optimization algorithm, a hull surface deformation method, and performance evaluation. Optimization parameters and constraints link the algorithm and the deformation method. The deformation method transfers hull data to performance evaluation software (e.g., CFD, FEA solvers) for computation. Finally, the objective function from the performance evaluation is fed back to the optimization algorithm for automated optimization [1].

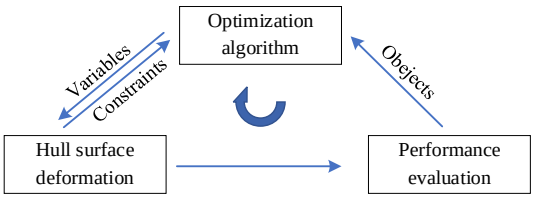


Figure 1. SBD-based ship optimization framework.

Check for updates

Academic Editor: Tamara Nestorović

Received: 3 June 2026
Revised: 1 July 2026
Accepted: 6 July 2026
Published: 10 July 2026

Copyright: © 2026 by the authors. Licensee MDPI, Basel, Switzerland. This article is an open access article distributed under the terms and conditions of the Creative Commons Attribution (CC BY) license.

To enhance optimization efficiency and quality, numerous scholars have conducted research, leading to three main categories of methods: (1) dimensionality reduction methods, which simplify variables to reduce problem dimensions (e.g., Karhunen–Loève Expansion (KLE), Sobol's sensitivity analysis); (2) approximation techniques, which use fast-response surrogate models instead of time-consuming simulations (e.g., Kriging models, Radial Basis Functions, Adaptive Neural Networks); (3) efficient optimization algorithms designed for rapid convergence (e.g., Genetic Algorithms, Ant Colony Optimization, Particle Swarm Optimization).

Extensive research has yielded fruitful results. Kim et al. [2] parametrically modeled a VLCC, using bow and stern feature parameters as optimization variables, and optimized wave resistance and viscous pressure resistance using Sequential Quadratic Programming (SQP) and deterministic particle swarm optimization, respectively. Campana et al. [3] applied KLE for dimensionality reduction in a high-speed catamaran optimization, selecting four parameters to control hull deformation, thereby reducing average total resistance in irregular waves at varying speeds. Jung et al. [4] performed multi-objective total resistance optimization for a KVLCC2 ship in waves, identifying principal dimensions, prismatic coefficient, and longitudinal center of buoyancy positions for improved resistance. Kim et al. [5] used longitudinal deformation and Free-Form Deformation (FFD) for a tanker, optimizing its resistance performance. Zakerdoost et al. [6] calculated hydrodynamic performance using a panel method and optimized Series 60 and Series 175 hulls. Nazemian et al. [7] used the Lackenby method to optimize the main and side hull profiles of a trimaran, followed by optimizing their relative positions. Heo et al. [8] combined CAESES and Wasim software to optimize KVLCC2 resistance in calm water and waves. Grigoropoulos et al. [9] integrated parametric modeling, genetic algorithms, and artificial neural networks into an optimization framework for the bow and stern shapes of the KCS ship. Park et al. [10] used the SQP algorithm to minimize the total resistance coefficient of the KCS. Renaud et al. [11] employed three approximate models to optimize seakeeping and drag performance for small waterplane area catamarans. Samuel et al. [12] optimized the total resistance of a frigate using bulbous bow shape parameters and analyzed the influence of the bulbous bow upturn angle.

In the aforementioned studies, optimization parameters serve as the bridge connecting the hull geometry and the optimization algorithm. During optimization, the algorithm continuously adjusts these parameters to achieve geometric deformation of the hull surface. Therefore, the rationality of parameter selection critically determines the quality, and even the success, of the optimization results. However, determining the optimal number and spatial distribution of parameters to maximize the design space effectively remains a key challenge in hull form optimization. Currently, parameter selection primarily relies on design experience, which is subjective and inconsistent. To address this issue, this paper takes the KCS container ship as a case study to investigate optimization parameter selection methods and applies the findings to container ship optimization. This paper is structured as follows: Section 1 introduces the topic; Section 2 studies the influence of the number and distribution of optimization parameters; Section 3 investigates the effect of hull surface deformation degree on wave-making resistance; Section 4 proposes a parameter selection method based on surface strain energy; Section 5 applies the method to hull form optimization; and Section 6 provides a summary.

2. The Influence of the Number and Distribution Position of Optimization Parameters on Hull Form Optimization Results

2.1. Optimization Problem Description

The ITTC-recommended KCS container ship is used as the test case to explore the effects of optimization parameter number, distribution, and hull surface deformation on

wave-making resistance. The main particulars of the KCS are listed in Table 1, and a three-dimensional side view is shown in Figure 2.

Table 1. Main parameters.

Molded Volume (∇)	Length (Lpp)	Length of Waterline (Lwl)	Beam (Bwl)	Depth (D)	Draught (T)	Block Coefficient (Cb)
1.649 m^3	7.2786 m	7.2944 m	1.019 m	0.6013 m	0.3418 m	0.651



Figure 2. Three-dimensional side view of KCS.

The Radial Basis Function (RBF) interpolation method was used for hull surface modification, as detailed in references [13,14].

2.1.1. Optimization Objective

The objective is to minimize the wave-making resistance coefficient at the design speed (Fr = 0.26). The mathematical formulation is:

$$\min f_{obj} = C_w \quad F_r = 0.26 \tag{1}$$

Wave-making resistance is calculated using SHIPFLOW software.

2.1.2. Constraints

Fixed points during optimization are located along the bottom centerline, deck edge, forecastle leading edge, and near the midship section, as shown in Figure 3. Hydrostatic constraints are also applied:

1. longitudinal position of center of buoyancy $\frac{|L_{cb}-L_{cbopt}|}{L_{cb}} \leq 1\%$
2. Molded volume $0 \leq \frac{\nabla_{opt}-\nabla}{\nabla} \leq 10\%$

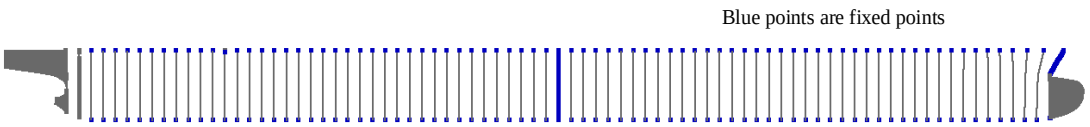


Figure 3. Distribution of fixed points of KCS.

Where ∇ is molded volume of the initial ship and ∇_{opt} is molded volume of the optimized ship. L_{cb} is the longitudinal position of the initial ship's center of buoyancy, and L_{cbopt} is the longitudinal position of the optimized ship's center of buoyancy.

2.1.3. Resistance Simulation Validation

SHIPFLOW software was used to calculate the resistance of the KCS at Fr = 0.26. Results were compared with experimental data to validate the numerical simulation accuracy, establishing a reliable foundation for subsequent studies.

The computational domain division and boundary condition settings for the KCS are as follows:

1. **Division of Wave-Making Resistance Computational Domain**

The division of the wave-making resistance computational domain is shown in Figure 4. Along the ship length direction, the domain extends 0.5 times the ship length (L) upstream from the bow and 1.0 L downstream from the stern. In the ship width direction, the domain extends outward by 0.7 L.

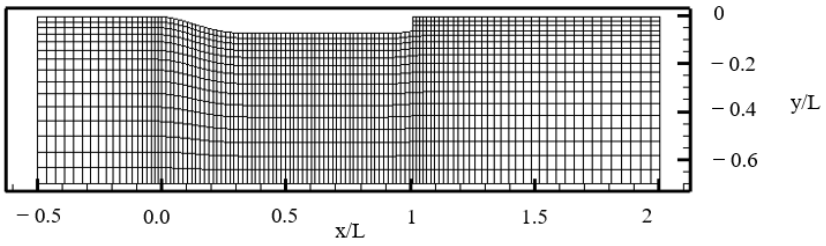


Figure 4. Wave-making resistance computational domain.

2. Division of Viscous Resistance Computational Domain

The division of the viscous resistance computational domain is shown in Figure 5. The coordinate origin is defined at the intersection of the waterline plane, the ship's longitudinal center plane, and the stem. The computational domain comprises one-quarter of a cylindrical fluid region with a radius of 3 L on one side of the hull. The ship's longitudinal center plane coincides with the symmetry plane. The bow is positioned 0.5 L from the inflow boundary, and the stern is 1 L from the outflow boundary. The mesh configuration is 159 × 70 × 100 (axial × circumferential × radial), totaling approximately 1.11 million grids.

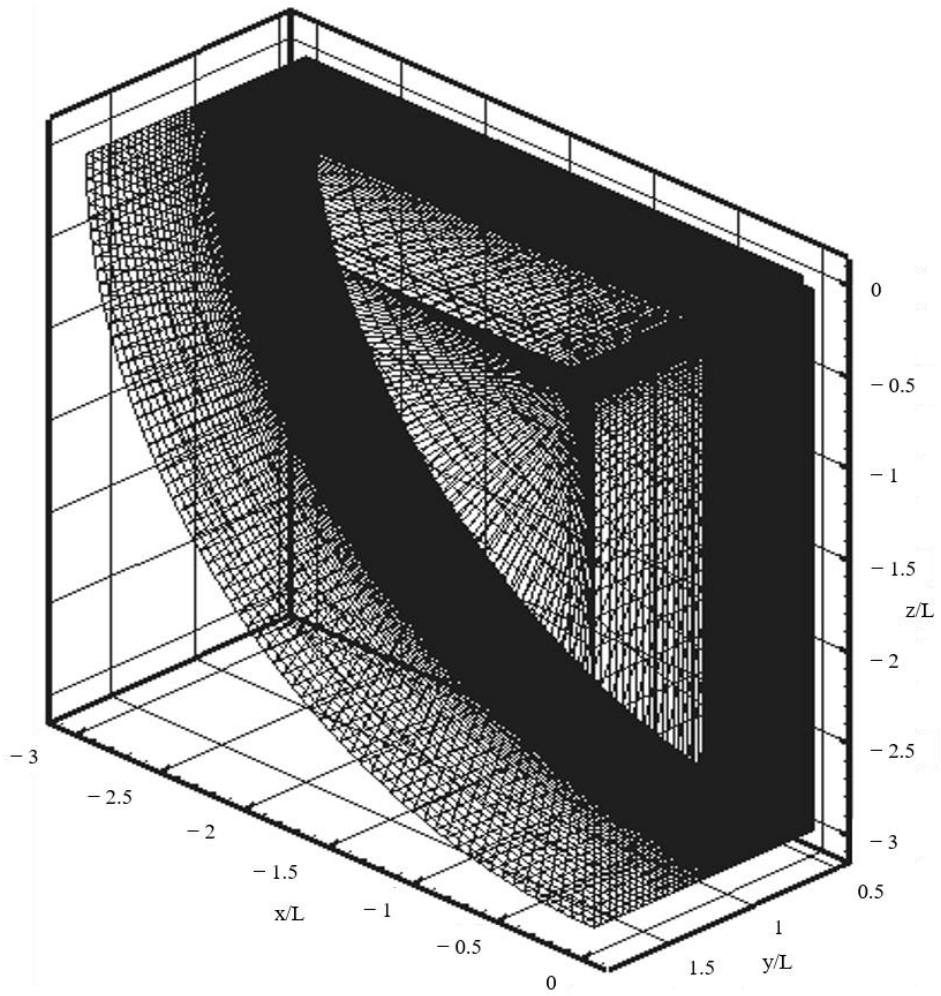


Figure 5. Viscous resistance computational domain.

3. Boundary Condition Settings for Viscous Resistance Calculation

Inflow boundary: set as an inflow boundary condition.

Outflow boundary: defined as an outflow boundary condition.

Outer boundary and symmetry plane: assigned a slip condition.

Hull surface: treated as a solid wall with a no-slip wall condition.

A comparison between the SHIPFLOW numerical simulation results and experimental data is presented in Table 2.

Table 2. Comparison of SHIPFLOW simulation results with experimental data.

	$C_t \times 10^3$	$C_f \times 10^3$	$C_r \times 10^3$
Experiment	3.56	2.83	0.731
SHIPFLOW	3.555	2.745	0.810

C_t denotes the total resistance coefficient, C_f represents the frictional resistance coefficient, C_r indicates the residual resistance coefficient (comprising wave-making resistance and vortex-induced resistance).

The experimental results measure the total resistance coefficient C_t, while the frictional resistance coefficient C_f is derived through integration using the flat-plate formula. The residual resistance coefficient C_r is obtained by subtracting C_f from C_t. In contrast, the SHIPFLOW software calculates both the total resistance coefficient C_t and the wave-making resistance coefficient C_w.

Analysis of Table 2 reveals that the error between the SHIPFLOW-calculated total resistance and experimental results is merely 0.14%, which meets the requirements for engineering applications. This demonstrates the high reliability of SHIPFLOW for total resistance simulations. However, due to methodological differences in resistance decomposition, the reliability of the wave-making resistance simulation cannot be directly assessed using the data in Table 2.

To further validate the accuracy of the wave-making resistance simulation, the numerically simulated wave patterns and wave height distributions of the KCS hull form are compared with experimental measurements, as shown in Figures 6 and 7. A detailed comparison of the wave contour lines in Figure 6 indicates excellent agreement between the simulation and experimental results at key locations, including the bow, stern, and shipside wave crests/troughs. This confirms that SHIPFLOW can accurately simulate wave generation at the bow and stern regions.

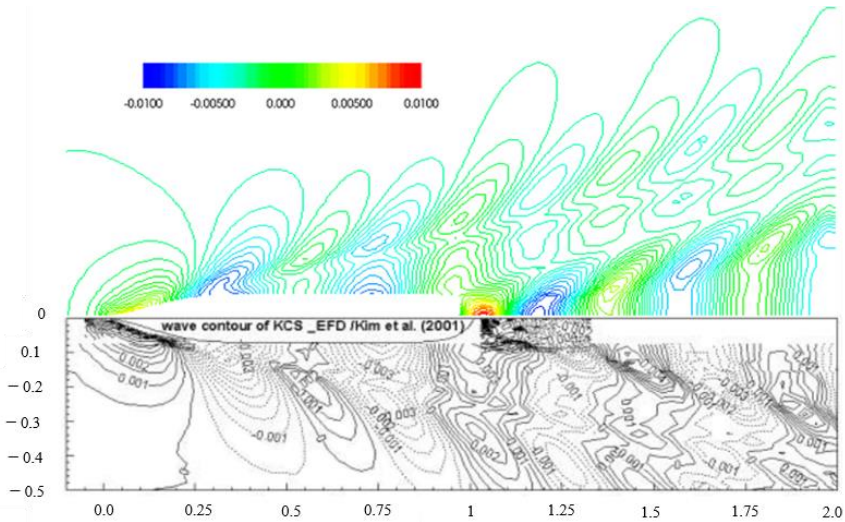


Figure 6. Wave pattern comparison of the KCS hull form (top: mumerical simulation; bottom: experiment [15]).

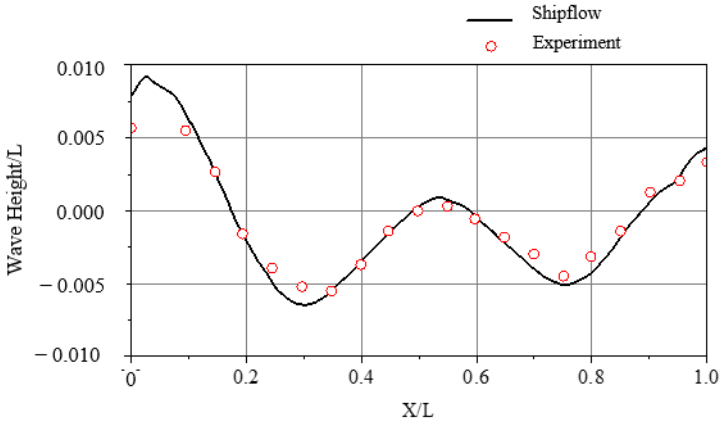


Figure 7. Longitudinal wave height profile of the KCS hull form at Y/L = −0.1509 $Y/L = -0.1509$.

As shown in Figure 7, the numerical simulation results closely align with the experimental wave height trends from the bow to 1 L. The simulation accurately captures the positions of wave crests/troughs and the magnitudes of wave amplitudes.

Through the comparison of numerical simulations and experimental results, it is sufficiently demonstrated that SHIPFLOW achieves engineering-grade precision in predicting both wave-making resistance and total resistance, confirming its high reliability for practical applications. This conclusion establishes a robust foundation for the subsequent investigation into how the number and distribution of optimization parameters influence the resistance performance of the hull form.

2.2. The Influence of the Number of Optimization Parameters on the Ship Form Optimization Results

When exploring the influence of the number of parameters on the optimization of wave-making resistance, the optimization points should be selected first, and then the optimization parameters should be determined according to the optimization points.

The distribution of optimization points is shown in Figure 4. Distribute fixed points in the middle of the hull profile (as shown in the blue square) to ensure that the hull profile and parallel hull do not change and distribute optimization points in the bow of the hull (as shown in red). In this paper, the most forward point ($\mathbf{P}_1$) on the bulbous bow is selected as the first optimization point. The X coordinate and Z coordinate of $\mathbf{P}_1$ are variables so that the shape of the bulbous bow can change along the length and depth direction. Point $\mathbf{P}_2$ is also distributed on the bulbous bow and works together with P1 to increase the complexity of bulbous bow deformation. Point $\mathbf{P}_3$ is located near the waterline near the bow of the bulb. Point $\mathbf{P}_4$ is distributed near the waterline close to the parallel midbody and works with $\mathbf{P}_3$ to change the fullness of the waterline to affect the wave-making resistance optimization. Point $\mathbf{P}_5$ is distributed at the transition from parallel center body to bow, which can change the length of the inlet section. Point $\mathbf{P}_6$ is distributed in the bow. The coordinates of the optimization points $\mathbf{P}_2$~$\mathbf{P}_6$ change along the Y (ship width) direction.

According to the distribution of optimization points in Figure 8, this paper designs six optimization cases, as shown in Table 3. In Case 1, there is only $\mathbf{P}_1$ point, including two optimization parameters. In Case 2, point $\mathbf{P}_2$ is added based on Case 1, and the corresponding optimization parameters are as follows: Case 3 adds point P3 based on Case 2, and the corresponding increase in optimization parameters, and so on. The variation range of optimization parameters is determined according to design experience. In this example, all optimization parameters vary within ±5%. The number of optimization parameters in each case and their variation range are shown in Table 3.

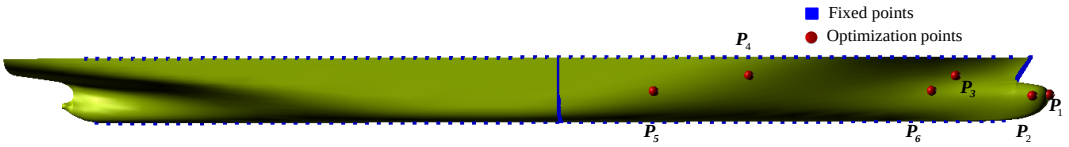


Figure 8. Fixed and optimization points distribution of KCS.

Table 3. The number of optimization parameters in each scheme and their variation range.

Case	Optimization Points and Parameters						Range/m
1	$\mathbf{P}_1$ (x_1,z_1)						$-0.1 \leq x_1 \leq 0.002$ $-0.1854 \leq x_1 \leq 0.2049$
2	$\mathbf{P}_1$ (x_1,z_1)	$\mathbf{P}_2$ (y_2)					x_1, z_1 as above. $-0.0701 \leq y_2 \leq 0.0774$
3	$\mathbf{P}_1$ (x_1,z_1)	$\mathbf{P}_2$ (y_2)	$\mathbf{P}_3$ (y_3)				x_1, z_1, y_2 as above. $-0.0776 \leq y_3 \leq 0.0858$
4	$\mathbf{P}_1$ (x_1,z_1)	$\mathbf{P}_2$ (y_2)	$\mathbf{P}_3$ (y_3)	$\mathbf{P}_4$ (y_4)			x_1, z_1, y_2, y_3 as above. $-0.1044 \leq y_4 \leq 0.1154$
5	$\mathbf{P}_1$ (x_1,z_1)	$\mathbf{P}_2$ (y_2)	$\mathbf{P}_3$ (y_3)	$\mathbf{P}_4$ (y_4)	$\mathbf{P}_5$ (y_5)		x_1, z_1, y_2, y_3, y_4 as above. $-0.4750 \leq y_5 \leq 0.5250$
6	$\mathbf{P}_1$ (x_1,z_1)	$\mathbf{P}_2$ (y_2)	$\mathbf{P}_3$ (y_3)	$\mathbf{P}_4$ (y_4)	$\mathbf{P}_5$ (y_5)	$\mathbf{P}_6$ (y_6)	x_1, z_1, y_2, y_3, y_4, y_5 as above. $-0.4500 \leq y_6 \leq 0.4973$

SHIOMDO-WUT, a multi-disciplinary comprehensive optimization platform for ship hydrodynamic performance developed by our team, was used to optimize the hull form of each case. In this example, SHIPFLOW software is used to calculate the wave-making resistance, the fluid domain around the ship into potential basin, and boundary layer region and viscous basin according to the characteristics of the flow field; adopts different methods to ensure the calculation accuracy; and greatly reduces the calculation cost. In this example, the calculation domain of the wave resistance is 0.7 length outward from the side, 0.5 length upstream from the bow longitudinally, and 1 length downstream from the stern of the ship. The calculation grid adopts medium (medium) density grid, and the number of grids is 744,000. Particle swarm optimization (PSO) is used to carry out iterative optimization. PSO is a global optimization algorithm, which has the characteristics of fast speed and good robustness for solving multi-dimensional space functions and dynamic target optimization problems. The particle number, optimization algebra settings, and optimization solutions of the PSO algorithm in each scheme are shown in Table 4. The main performance parameter pairs between the optimized hull form and the initial ship type are shown in Table 5

Table 4. Optimized solutions and particle swarm optimization settings.

	x_1	z_1	y_2	y_3	y_4	y_5	y_6	Particle Number	Optimization Algebra
Case 1	−0.07974	0.1989						40	22
Case 2	−0.07974	0.1989	0.07007					60	20
Case 3	−0.07974	0.1989	0.07007	0.08577				60	20
Case 4	−0.07974	0.1989	0.07007	0.08577	0.4735			60	30
Case 5	−0.07974	0.1989	0.07007	0.08577	0.4735	0.5095		60	30
Case 6	−0.07974	0.1989	0.07007	0.08577	0.4735	0.5095	0.1108	60	40

Table 5. Comparison of optimized ship of each case and the initial ship (model-scale).

	∇	L_{cb}	Wetted Surface	$C_w \times 10^3$	Change (C_w)	Wave-Making Resistance
Initial ship	1.648 m^3	3.969 m	9.538 m^2	0.5739	0	50.8201 N
Case 1	1.649 m^3	3.965 m	9.579 m^2	0.5561	−2.6851%	49.4555 N
Case 2	1.649 m^3	3.964 m	9.569 m^2	0.5363	−6.2479%	47.6449 N
Case 3	1.649 m^3	3.966 m	9.569 m^2	0.5309	−7.1919%	47.1651 N
Case 4	1.648 m^3	3.964 m	9.565 m^2	0.5321	−7.0210%	47.2520 N
Case 5	1.672 m^3	3.959 m	9.651 m^2	0.5238	−7.6484%	46.9331 N
Case 6	1.671 m^3	3.962 m	9.648 m^2	0.5238	−7.6771%	46.9186 N

The wave-making resistance changes between the optimized ship (black dot) and the initial ship (red dot) of each case are plotted in Figure 9 (the horizontal coordinate indicates the schemes, and the vertical coordinate indicates the wave-making resistance). According to the results, with the increase in optimization parameters, the hull surface becomes more and more complex and the wave-making resistance of the optimized ship decreases. Therefore, the quality of hull form optimization can be improved by appropriately increasing the number of optimization parameters. It can also be found that when the optimization parameters are distributed in the position of the bulbous bow, the wave-making resistance of the optimized ship decreases greatly. When the distribution position of optimization parameters in the bow is unreasonable, the amplitude of the wave resistance decreases significantly, and even the wave resistance increases with the increase in the number of optimization parameters. Therefore, it is necessary to further study the influence of the distribution position of optimization parameters on optimization.

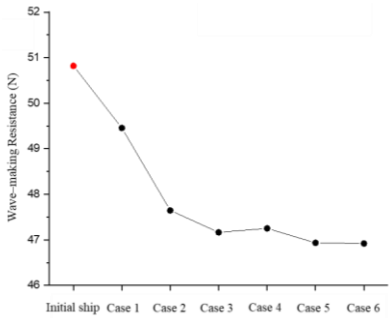


Figure 9. The wave-making resistance of the initial ship and the optimized ship.

2.3. Influence of Distribution of Optimization Parameters on Wave-Making Resistance

To facilitate the description of the distribution position of optimization parameters, the hull surface of KCS is divided into four areas (Area 1, 2, 3, 4), as shown in Figure 10, and the influence of optimization parameters distribution in these areas on the wave-making resistance performance of ships is explored.



Figure 10. Four-area division of KCS.

The four areas in Figure 10 are described below:

Area 1: bulbous bow position before bow-vertical line.

Area 2: the side of the bow above the bilge, below the waterline, and before the parallel midbody.

Area 3: the bilge area before the parallel midbody of the ship.

Area 4: aft area of the ship after the parallel midbody, before the stern vertical line, and below the waterline.

According to the distribution area of optimization parameters determined in Figure 11, this section designs four cases of optimization parameter distribution, as shown in Table 6. In the table, "√" indicates that optimization parameters are distributed in this region and RBF deformation occurs in this region, and "×" indicates that there is no optimization parameter distribution in this region and no deformation occurs in this region.

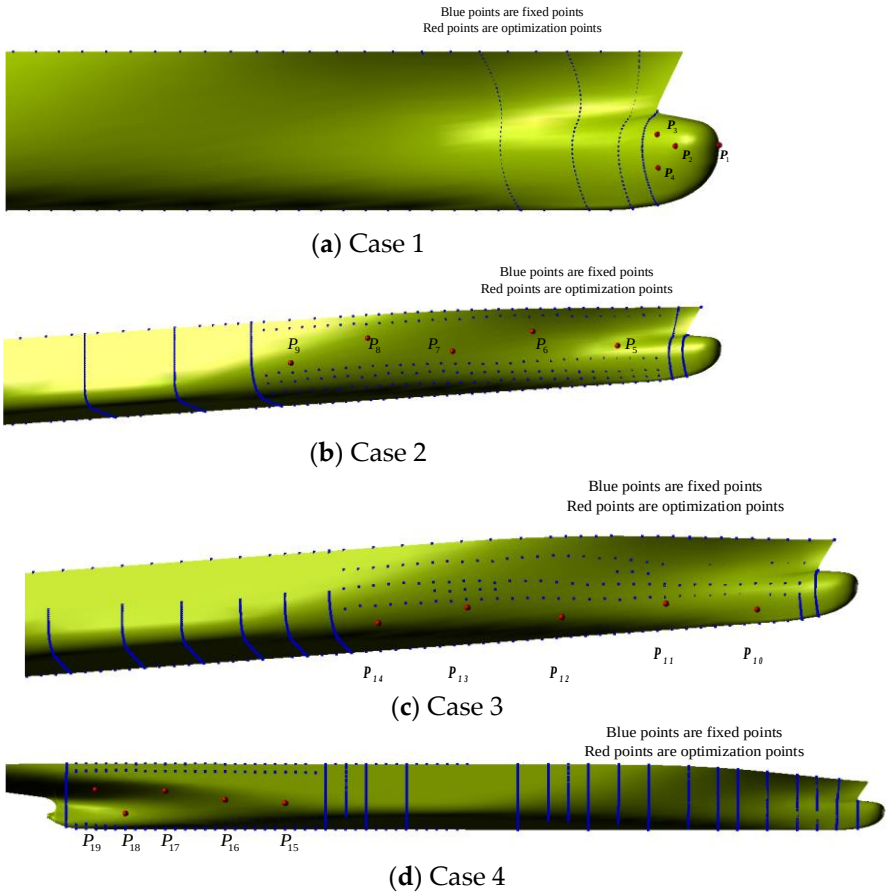


Figure 11. Distribution of optimization points and fixed points on KCS.

Table 6. Cases division.

Case	Area 1	Area 2	Area 3	Area 4
1	√	×	×	×
2	×	√	×	×
3	×	×	√	×
4	×	×	×	√

When exploring each case, the distribution of optimization points is first determined, as shown in Figure 11.

When determining the variation range of optimization parameters, the following constraints should be met: (1) the variation range of optimization parameters in each area should not exceed the maximum half-width of the hull; (2) the variation range of optimization parameters in each region along the Y (ship width) direction should be the same. Considering the particularity of the optimization point P1, the variation range of the corresponding optimization parameters is determined separately according to design experience. The optimization parameters and their variation range in each scheme are shown in Table 7.

Table 7. Optimization parameters in each scheme and their variation range.

	Optimization Points	Optimization Parameters	Initial Value	Upper	Lower
Case 1	$\mathbf{P}_1$	x_1	−0.000210	0.000200	−0.005000
		z_1	0.195157	0.204915	0.185399
	$\mathbf{P}_2$	y_2	0.073668	0.094080	0.053320
	$\mathbf{P}_3$	y_3	0.069144	0.089480	0.048720
	$\mathbf{P}_4$	y_4	0.064730	0.085080	0.044320
Case 2	$\mathbf{P}_5$	y_5	0.084749	0.105080	0.064320
	$\mathbf{P}_6$	y_6	0.242951	0.263380	0.222620
	$\mathbf{P}_7$	y_7	0.330939	0.351280	0.310520
	$\mathbf{P}_8$	y_8	0.479313	0.499693	0.458933
	$\mathbf{P}_9$	y_9	0.486762	0.507180	0.466420
Case 3	$\mathbf{P}_{10}$	y_{10}	0.049540	0.069880	0.029120
	$\mathbf{P}_{11}$	y_{11}	0.135460	0.155880	0.115120
	$\mathbf{P}_{12}$	y_{12}	0.211877	0.232280	0.191520
	$\mathbf{P}_{13}$	y_{13}	0.367500	0.387880	0.347120
	$\mathbf{P}_{14}$	y_{14}	0.390907	0.411280	0.370520
Case 4	$\mathbf{P}_{15}$	y_{15}	0.466111	0.486480	0.445720
	$\mathbf{P}_{16}$	y_{16}	0.421246	0.441580	0.400820
	$\mathbf{P}_{17}$	y_{17}	0.418385	0.438780	0.398020
	$\mathbf{P}_{18}$	y_{18}	0.123888	0.144280	0.103520
	$\mathbf{P}_{19}$	y_{19}	0.304366	0.324780	0.284020

In each case, 5 optimization parameters are selected as variables, and 100 hull form samples are generated by uniform experimental design under the condition of ensuring the calculation accuracy.

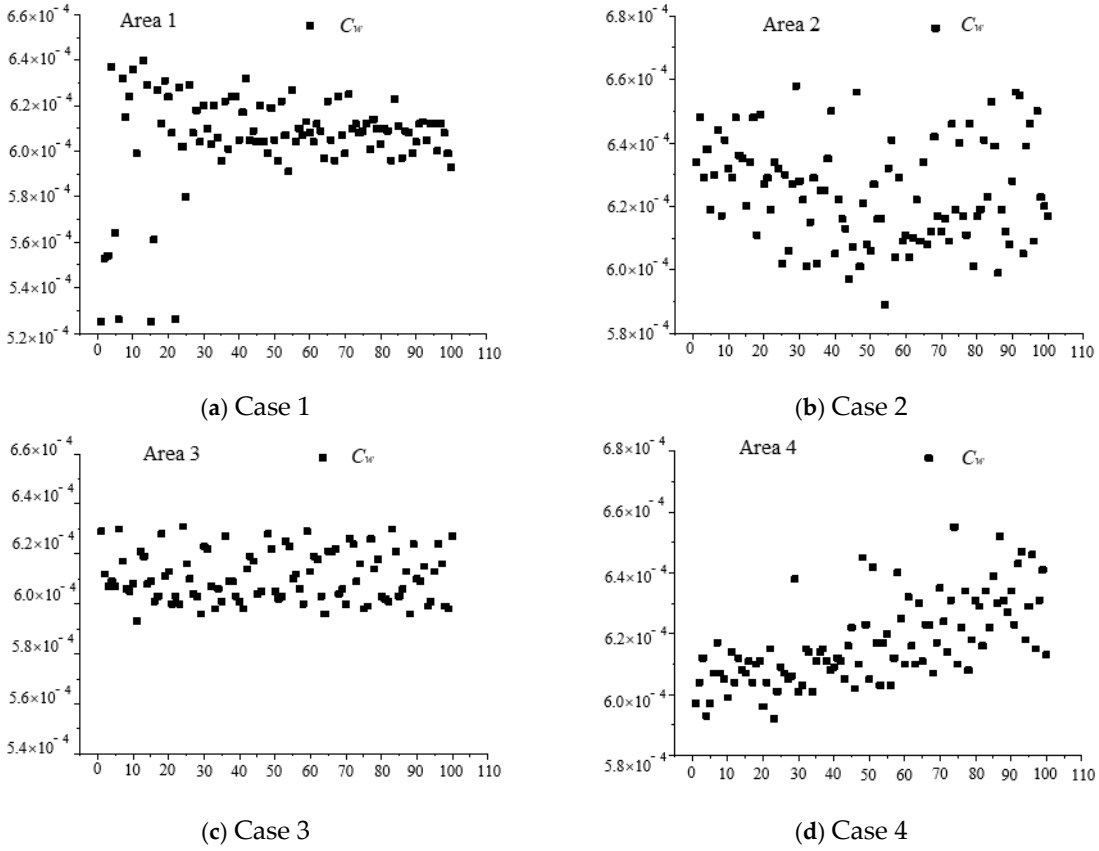
The wave-making resistance coefficients of the samples are expanded along the sample number, as shown in Figure 12, to intuitively analyze the changes of wave-making resistance.

It can be intuitively found from Figure 12 that when the optimization parameters are distributed in the bulbous bow (Case 1), the wave-making resistance coefficient fluctuates sharply. When the optimization parameters are distributed in the bilge region (Case 3), the wave-making resistance coefficient fluctuates the most gently and the fluctuation range is the smallest, indicating that the optimization parameters distributed in this region have no obvious influence on the resistance.

The concept of sample variance in statistics is used to quantitatively analyze the dispersion degree of the wave-making resistance coefficient of the samples in each scheme, and the dispersion degree is used to represent the influence degree of the optimization parameter distribution region on the optimization of ship wave-making resistance. The more drastic the fluctuation of the wave-making resistance coefficient of the samples, the more obvious the influence of the optimization parameters distributed in this region on the wave-making resistance optimization. In statistics, sample variance S^2 is commonly used to describe the degree of dispersion of a group of data, and its calculation formula is as follows:

$$S^2 = \frac{1}{n-1}\sum_{i=1}^{n}(y_i - \overline{y})^2 \tag{2}$$

where n is the number of samples, y_i is the wave-making resistance coefficient of each ship type sample point, and $\overline{y}$ is the average wave-making resistance coefficient of samples.



(**a**) Case 1 (**b**) Case 2

(**c**) Case 3 (**d**) Case 4

Figure 12. Wave-making resistance coefficients of samples.

The variance of wave-making resistance coefficient of 100 samples in each case is shown in Table 8.

Table 8. The variance of 100 samples.

Name	Variance (S^2)
Case 1	1.43×10^{-9}
Case 2	2.52×10^{-10}
Case 3	1.27×10^{-10}
Case 4	1.90×10^{-10}

The data in Table 8 can be easily obtained as follows: $S^2_{\text{Case1}} > S^2_{\text{Case2}} > S^2_{\text{Case4}} > S^2_{\text{Case3}}$. According to the degree of influence of the optimized parameter distribution region on the optimization of wave-making resistance, the optimized parameter distribution region can be sorted as follows: bulbous bow region > bow side region > stern region > bilge region, which is consistent with the distribution of wave-generating resistance coefficients of the sample points of each scheme in Figure 12.

3. Influence of Surface Deformation Degree on Wave-Making Resistance

According to the research in Part 2, it is helpful to obtain a better potential design scheme when the optimization parameters are centrally arranged to the bulbous bow and bow side region of hull form optimization. However, the problem of how to select optimization parameters in these parts has not been solved. Considering that when the hull surface is deformed geometrically, it is usually required to use as few parameters as possible (that is, optimization parameters) to make the ship change as large as possible to produce different types of ship shapes. This part explores how to select the optimization parameters

from the perspective of ship geometric deformation, proposes to use the strain energy of the surface to describe the deformation degree of the surface, and further explores the influence of the deformation degree of the surface on the optimization of ship wave resistance.

3.1. Strain Energy Calculation of Surface

3.1.1. Calculation and Derivation of Strain Energy of Surface

The strain energy of a surface can be calculated from two aspects, one is the physical deformation energy, the other is the geometric deformation. In this paper, the strain energy of the surface is calculated from the point of view of physical deformation energy. It is generally believed that parametric surfaces $S : \Omega \to R^3$ contain two parts of energy: bending resistance and tensile resistance, and the strain energy $E_{deformation}$ of the surface can be expressed as:

$$E_{deformation} = \int_{\sigma} \left(\alpha E_{stretch} + \beta E_{bending} \right) d\sigma \tag{3}$$

where α and β are the weight coefficients, $E_{stretch}$ is the tensile energy, $E_{bending}$ is the bending energy, and $E_{deformation}$ is the strain energy of the surface, that is, the energy of the surface.

Using the elastic deformation equation of a thin plate in elasticity mechanics, the energy of the surface is expressed in the following [16]:

$$\begin{aligned} E(S) = \quad & \iint [\alpha_{11} S_{\mu}^2 + 2\alpha_{12} S_{\mu} S_{\nu} + \alpha_{22} S_{\nu}^2 + \beta_{11} S_{\mu\mu}^2 + \\ & 2\beta_{12} S_{\mu\nu}^2 + \beta_{22} S_{\nu\nu}^2 - 2Sf(\mu, \nu)] d\mu d\nu \end{aligned} \tag{4}$$

In Formula (4), S is the desired surface with parameters μ and ν, S_{μ} and S_{ν} are the first partial derivatives of the surface along directions μ and ν, $S_{\mu\mu}$ and $S_{\nu\nu}$ are the second partial derivatives along directions μ and ν, and $S_{\mu\nu}$ is the mixed partial derivatives of the surface. α and β are material property coefficients, α is related to the area change of the energy surface, β is related to the curvature change of the energy surface; f is the vector function of the given external load.

In this paper, the energy of a surface expressed as a B-spline under no load is discussed. B-spline surface is widely used in geometric modeling design, and its mathematical expression is as follows [17]:

$$S(\mu, \nu) = \sum_{i=0}^{n} \sum_{j=0}^{m} N_{i,p}(\mu) N_{j,q}(\nu) \mathbf{P}_{i,j}, \quad \leq \mu, \nu \leq 1 \tag{5}$$

In Formula (5), $\mathbf{P}_{i,j}$ is the control polygon vertex of surface $S(\mu, \nu)$, n and m are the number of control vertices of surface $S(\mu, \nu)$ in directions μ and ν, respectively, p and q are the power of surface $S(\mu, \nu)$ in directions μ and ν, respectively, and $N_{i,p}(\mu)$ and $N_{j,q}(\nu)$ are the node vectors defined in aperiodic directions, respectively

$$U = \{0, \ldots, 0, \mu_{p+1}, \mu_{p+2}, \ldots, \mu_{r-p-1}, 1, \ldots, 1\}, (r = n + p + 1)$$

and

$$V = \{0, \ldots, 0, \nu_{q+1}, \nu_{q+2}, \ldots, \nu_{s-q-1}, 1, \ldots, 1\}, \quad (s = m + q + 1)$$

The recursive expression of the non-rational B-spline basis function is as follows:

$$\begin{aligned} N_{i,p}(\mu) &= \frac{\mu - \mu_i}{\mu_{i+p} - \mu_i} N_{i,p-1}(\mu) + \frac{\mu_{i+p+1} - \mu}{\mu_{i+p+1} - \mu_{i+1}} N_{i+1,p-1}(\mu) \\ N_{i,0}(\mu) &= \begin{cases} 1, & \mu_i \leq \mu \leq \mu_{i+1} \\ 0, & \text{other} \end{cases} \end{aligned} \tag{6}$$

The expressions of the first partial derivatives S_μ and S_ν, the second partial derivatives $S_{\mu\mu}$ and $S_{\nu\nu}$, and the mixed partial derivatives $S_{\mu\nu}$ of the surface $S(\mu,\nu)$ are as follows:

$$S_\mu(\mu,\nu) = \sum_{i=0}^{n}\sum_{j=o}^{m} N'_{i,p}(\mu)N_{j,q}(\nu)\mathbf{P}_{i,j} \tag{7}$$

$$S_\nu(\mu,\nu) = \sum_{i=0}^{n}\sum_{j=o}^{m} N_{i,p}(\mu)N'_{j,q}(\nu)\mathbf{P}_{i,j} \tag{8}$$

$$S_{\mu\mu}(\mu,\nu) = \sum_{i=0}^{n}\sum_{j=o}^{m} N''_{i,p}(\mu)N_{j,q}(\nu)\mathbf{P}_{i,j} \tag{9}$$

$$S_{\nu\nu}(\mu,\nu) = \sum_{i=0}^{n}\sum_{j=o}^{m} N_{i,p}(\mu)N''_{j,q}(\nu)\mathbf{P}_{i,j} \tag{10}$$

$$S_{\mu\nu}(\mu,\nu) = \sum_{i=0}^{n}\sum_{j=o}^{m} N'_{i,p}(\mu)N'_{j,q}(\nu)\mathbf{P}_{i,j} \tag{11}$$

Put Equation (7)–(11) into Equation (4), there is

$$\begin{aligned} E(S) = \int_0^1\int_0^1 \sum_{i=0}^{n}\sum_{j=0}^{m}\mathbf{P}_{i,j}\sum_{k=0}^{n}\sum_{l=0}^{m}\mathbf{P}_{k,l}[&\alpha_{11}N'_{i,p}(\mu)N_{j,q}(\nu)N'_{k,p}(\mu)N_{l,q}(\nu)\\ &+2\alpha_{12}N'_{i,p}(\mu)N_{j,q}(\nu)N_{k,p}(\mu)N'_{l,q}(\nu)\\ &+\alpha_{22}N_{i,p}(\mu)N'_{j,q}(\nu)N_{k,p}(\mu)N'_{l,q}(\nu)\\ &+\beta_{11}N''_{i,p}(\mu)N_{j,q}(\nu)N''_{k,p}(\mu)N_{l,q}(\nu)\\ &+2\beta_{12}N'_{i,p}(\mu)N'_{j,q}(\nu)N'_{k,p}(\mu)N'_{l,q}(\nu)\\ &+\beta_{22}N_{i,p}(\mu)N''_{j,q}(\nu)N_{k,p}(\mu)N''_{l,q}(\nu)]d\mu d\nu \end{aligned} \tag{12}$$

Let

$$\begin{aligned} S_{i,j,k,l} = {}&\alpha_{11}N'_{i,p}(\mu)N_{j,q}(\nu)N'_{k,p}(\mu)N_{l,q}(\nu) + 2\alpha_{12}N'_{i,p}(\mu)N_{j,q}(\nu)N_{k,p}(\mu)N'_{l,q}(\nu)\\ &+\alpha_{22}N_{i,p}(\mu)N'_{j,q}(\nu)N_{k,p}(\mu)N'_{l,q}(\nu) + \beta_{11}N''_{i,p}(\mu)N_{j,q}(\nu)N''_{k,p}(\mu)N_{l,q}(\nu)\\ &+2\beta_{12}N'_{i,p}(\mu)N'_{j,q}(\nu)N'_{k,p}(\mu)N'_{l,q}(\nu) + \beta_{22}N_{i,p}(\mu)N''_{j,q}(\nu)N_{k,p}(\mu)N''_{l,q}(\nu)]d\mu d\nu \end{aligned} \tag{13}$$

From Equation (13), using the property of integration, Equation (12) can be simplified into the following form:

$$E(S) = \sum_{\substack{i=0,n\\ j=0,m\\ k=0,n\\ l=0,m}} \left(\mathbf{P}_{i,j}\bullet\mathbf{P}_{k,l} \times S_{i,j,k,l}\right) \tag{14}$$

As long as the B-spline expression of the hull surface is determined, the strain energy of the hull surface can be calculated according to Equation (14).

3.1.2. B-Spline Surface Interpolation Fitting of Hull Form

In hull form optimization, it is usually difficult to obtain the B-spline surface expression of ship form directly. It is necessary to use parametric surface interpolation fitting or approximation fitting technology to generate the target surface from the discrete three-dimensional point cloud data so as to obtain the B-spline expression of the hull surface, that is, surface inversion [18,19].

The KCS used in this paper is composed of four B-spline surface slices. The three-dimensional discrete point clouds in each surface slice are regular gridded point clouds, and B-spline interpolation surfaces can be directly constructed by using point cloud data. The B-spline surface interpolation process is shown in Figure 13.

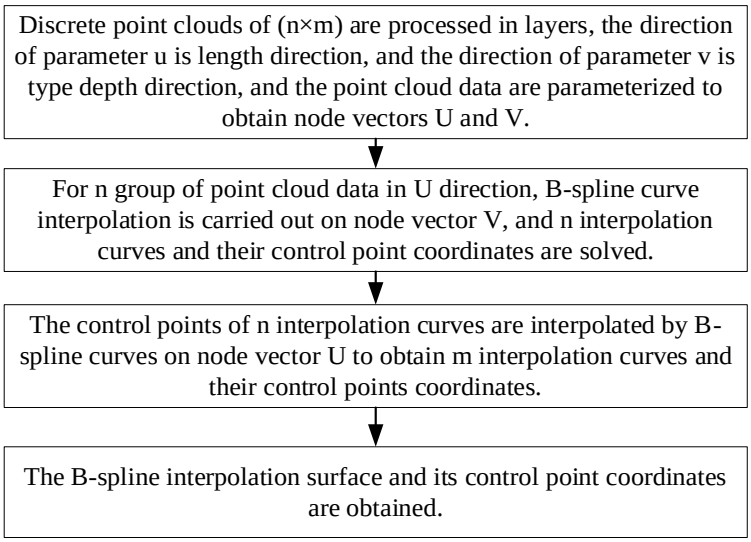


Figure 13. B-spline surface interpolation flow of KCS discrete point cloud.

In this example, it is necessary to fit the four surface slices of KCS by global surface interpolation. The B-spline surface interpolation fitting of the three-dimensional discrete point cloud of the KCS's bulbous bow surface is taken as an example to illustrate how to obtain the B-spline expression form of the ship curved surface. There is a total of 81 × 80 gridded point cloud data (81 in the u direction and 80 in the v direction) on the curved surface, as shown in Figure 14.

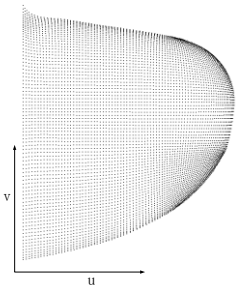


Figure 14. Three-dimensional discrete point cloud of the bulbous bow.

Step 1: the node vector U in the u direction and the node vector V in the v direction are obtained according to the three-dimensional point coordinates;

Step 2: 81 columns of three-dimensional point clouds are simulated to synthesize B-spline curves along the u direction, and the control point coordinates of each B-spline curve are stored in the array PC [].

Step 3: Along the v direction, 80 B-spline curves are synthesized from the control points on 81 B-spline curves obtained in step 2 to obtain a complete B-spline surface. The coordinates of the control points of the B-spline surface after fitting are stored in the array PS [].

Using the global surface interpolation and fitting technique, the B-spline surface of KCS ship shape bulbous bow was synthesized by the discrete point cloud, as shown in Figure 15.

The control point coordinates of the fitted surface and the node vectors in the direction of u and v are obtained by using the interpolation fitting technique. By bringing these parameters into Equation (14), the strain energy of the surface can be calculated.

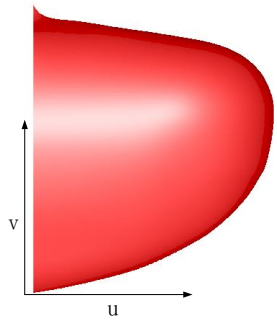


Figure 15. KCS bulbous bow interpolation fitted by B-spline surface.

3.2. Evaluation of Surface Deformation Based on Strain Energy

As can be seen from Equation (4), when calculating the strain energy of a continuously represented surface, the surface is usually required to be second-order faired. In this paper, a cubic B-spline basis function is used to ensure the continuous B-spline surface. Then, the strain energy calculation model of the surface is:

$$E(S) = \sum_{\substack{i=0,3 \\ j=0,3 \\ k=0,3 \\ l=0,3}} \left(\mathbf{P}_{i,j} \bullet \mathbf{P}_{k,l} \times S_{i,j,k,l} \right) \tag{15}$$

3.2.1. Evaluation Index of Surface Deformation Degree

According to the formula for solving the strain energy of a surface, it is easy to know that the coordinates of each point on the surface will change after the surface is deformed, and the strain energy of the surface will also change. Therefore, the strain energy of a surface can be used as an evaluation index to describe the deformation degree of a surface.

This section uses a simple example to verify the validity of the surface deformation evaluation index proposed in this paper.

Given a bicubic B-spline surface $S(u, v)$, the expression is:

$$S(\mu, \nu) = \sum_{i=0}^{3} \sum_{j=0}^{3} N_{i,3}(\mu) N_{j,3}(\nu) \mathbf{P}_{i,j}, \quad 0 \le \mu, \nu \le 1 \tag{16}$$

where $U = \{0, 0, 0, 0, 0.5013, 1, 1, 1, 1\}$, $V = \{0, 0, 0, 0, 1, 1, 1, 1\}$

There are 20 control vertices $\{\mathbf{P}_{i,j}\}$: $\mathbf{P}_{0,0}$ = (0.054505,0.040664, 0.120322), $\mathbf{P}_{0,1}$ = (0.051414, 0.051697, 0.14465), $\mathbf{P}_{0,2}$ = (0.046724, 0.064431, 0.190849), $\mathbf{P}_{0,2}$ = (0.046724, 0.064431, 0.190849), $\mathbf{P}_{0,3}$ = (0.048434, 0.058542, 0.227424), $\mathbf{P}_{1,0}$ = (0.083782, 0.048354, 0.115387), $\mathbf{P}_{1,1}$ = (0.08503, 0.062003, 0.146075), $\mathbf{P}_{1,2}$ = (0.086856, 0.076188, 0.189794), $\mathbf{P}_{1,3}$ = (0.086138, 0.069836, 0.230541), $\mathbf{P}_{2,0}$ = (0.125122, 0.054031, 0.106106), $\mathbf{P}_{2,1}$ = (0.124708, 0.070203, 0.147288), $\mathbf{P}_{2,2}$ = (0.12421, 0.076559, 0.189156), $\mathbf{P}_{2,3}$ = (0.124411, 0.070052, 0.232398), $\mathbf{P}_{3,0}$ = (0.16272, 0.055733, 0.10223), $\mathbf{P}_{3,1}$ = (0.162888, 0.071907, 0.148527), $\mathbf{P}_{3,2}$ = (0.163018, 0.07708, 0.188753), $\mathbf{P}_{3,3}$ = (0.163007, 0.070962, 0.232906), $\mathbf{P}_{4,0}$ = (0.201523, 0.56563, 0.098799), $\mathbf{P}_{4,0}$ = (0.201523, 0.56563, 0.09799), $\mathbf{P}_{4,1}$ = (0.201482, 0.07209, 0.149057), $\mathbf{P}_{4,2}$ = (0.201472, 0.077107, 0.188429), $\mathbf{P}_{4,3}$ = (0.20139, 0.070121, 0.23407).

The shape of the initial surface is shown in Figure 16a:

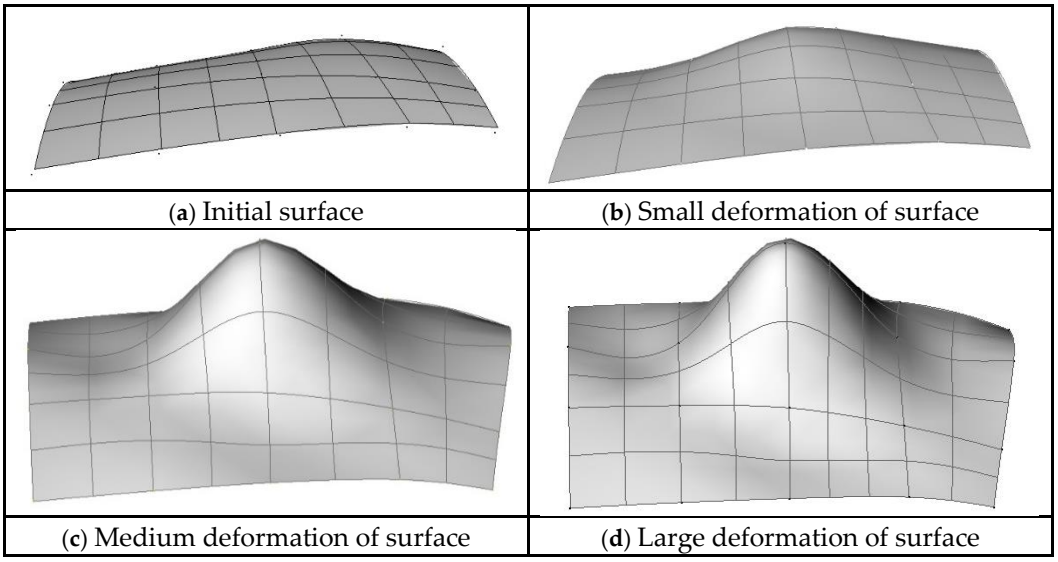


Figure 16. Comparison diagram of surface deformation degree.

Modify control points $P_{2,2}$ (0.12421, 0.076559, 0.209156). The surface shape is modified by the surface deformation method based on radial basis function interpolation. According to the principle of the deformation method, when the coordinates of point P2,2 change, the coordinates of the points around it within the support radius will change according to the interpolation equation. The entire surface is deformed accordingly, and the deformed surface is shown in Figure 16b.

Again, modify the control point $P_{2,2}$ (0.12421, 0.076559, 0.219156), the deformation of the curved surface is shown in Figure 16c. For the third revision control point P2,2 (0.12421, 0.076559, 0.229156), the deformation of the curved surface is shown in Figure 16d. The strain energy of the initial surface and the three deformed surfaces were calculated, respectively, as shown in Table 9:

Table 9. Deformation state of surface and corresponding strain energy of surface.

Surface	Strain Energy
Initial	2.3052
Small deformation	9.4081
Medium deformation	17.3394
Large deformation	26.8762

According to the observation and analysis of Figure 16 and Table 9 and the relevant knowledge of the strain energy of the surface, the strain energy of the surface changes with deformation of the surface. And the deformation degree of the surface is positively correlated with the strain energy of the surface. The greater the deformation of the surface, the greater the strain energy of the surface. Therefore, it is reasonable to use the strain energy of the surface to describe the deformation degree of the surface.

The hull surface is generally composed of several B-spline surfaces, so it is necessary to carry out further research when the strain energy of the hull surface is used as the evaluation index of the deformation degree of the hull surface.

3.2.2. Application of Surface Deformation Evaluation Index in Hull Surface Deformation

Taking the bulbous bow surface deformation of KCS as an example, the rationality of using strain energy of hull surface as an evaluation index of hull surface deformation degree is verified.

As shown in Figure 17, five optimization points P1~P5 were selected at the bulbous bow position, and the Y coordinate of each optimization point was taken as the optimization parameter y_1~y_5. According to experience, the value range of optimization parameters is set to ±10%. The uniform experimental design method in the optimization platform is used to generate 100 samples, among which 2 samples are selected. The values of optimization parameters are shown in Table 10.

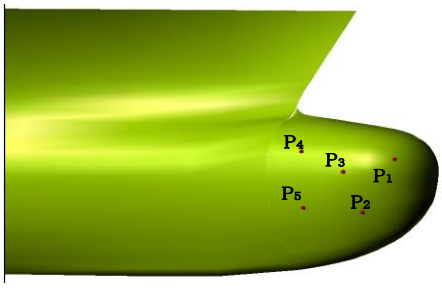


Figure 17. Optimization points at the bulbous bow of KCS.

Table 10. Values of optimization parameters in two samples.

	y_1	y_2	y_3	y_4	y_5
Initial ship	0.050884	0.051607	0.073668	0.069144	0.06473
Sample 1	0.045898	0.048219	0.069427	0.067398	0.06362
Sample 2	0.052272	0.054266	0.072748	0.069325	0.06388

The RBF is used to modify the hull surface. The comparison of the cross-section between the samples and the initial ship is shown in Figure 18.

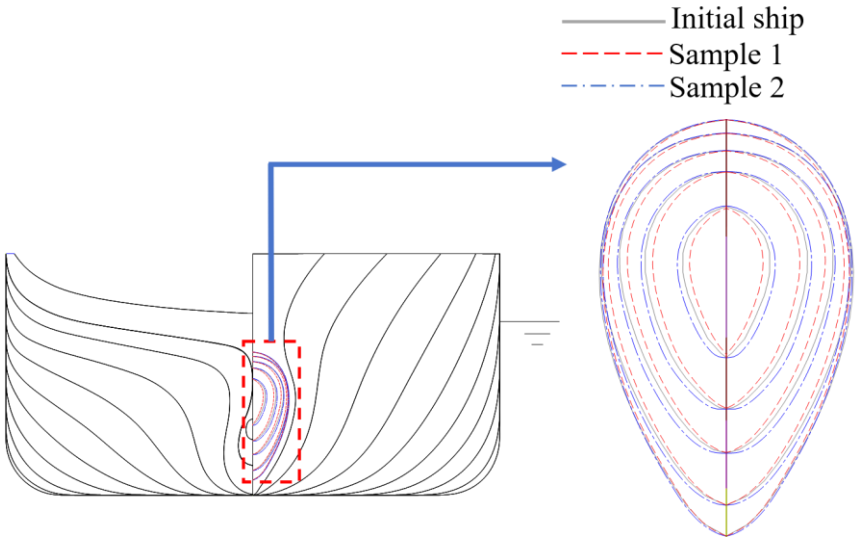


Figure 18. Cross-sectional comparison of samples and the initial ship.

The strain energy of the bulbous bow surface in the initial ship, Sample 1 and Sample 2, was calculated as shown in Table 11. Refer to Section 3.1 for the calculation principle. According to the analysis of Table 11, the strain energy after deformation of the bulbous bow surface is greater than that of the original ship's bulbous bow surface, and the strain energy of the bulbous bow surface sheet in Sample 1 is greater than that in Sample 2, indicating that the deformation degree of the hull surface in Sample 1 is greater than that in Sample 2. This is also illustrated by the cross-sectional comparison in Figure 18.

Table 11. Strain energy of bulbous bow surface in each scheme.

	Strain Energy
Initial ship	11,788
Sample 1	232,760
Sample 2	43,631

Therefore, it is reasonable to use the strain energy of the surface as the evaluation index of the deformation degree of the surface in this paper. This lays a foundation for the follow-up research.

3.3. Influence of Deformation Degree of Hull Surface on Wave-Making Resistance Optimization

According to the design experience, there are two main factors affecting the optimization of wave-making resistance of ships: (1) ship's length and prismatic coefficient (Cp); (2) the hull shape, especially the shape of the fore and stern part, will have an important impact on the optimization of wave-making resistance. However, during ship optimization, the main scale elements such as the length are generally fixed, and designers mainly reduce the resistance by changing the shape of the hull surface. Therefore, it is meaningful to study the influence of the hull shape on the wave-making resistance optimization with the help of the deformation degree of the hull surface and apply it to the hull form optimization.

In Section 2.3, the distribution of optimization parameters in the bulb bow area and the bow side area has a great influence on the wave-making resistance optimization. This section focuses on the influence of the deformation degree of the ship bow area on the wave-making resistance optimization. Five optimization parameters were selected in the bulbous bow area and the bow side area, and 100 samples were generated by the uniform experimental design method. The wave-making resistance coefficient corresponding to each sample was calculated by SHIPFLOW. The strain energy of the hull surface is calculated, and the strain energy of the surface is used as the index to evaluate the deformation degree of the hull surface.

The wave-making resistance coefficient and surface strain energy corresponding to samples in each region are drawn in the same diagram and are expanded according to the order of surface strain energy from small to large, as shown in Figure 19.

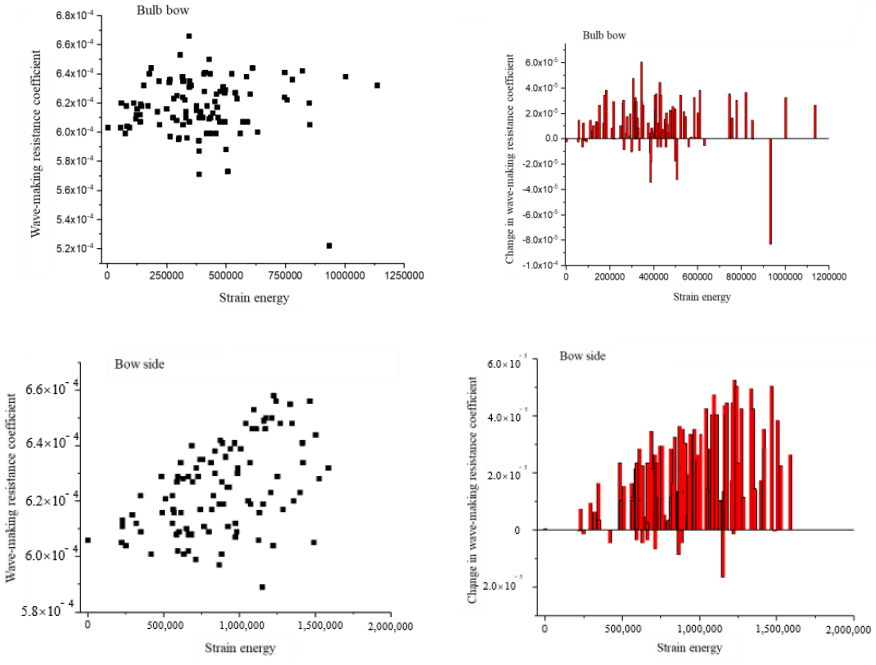


Figure 19. Distribution of wave-making resistance coefficients in different regions with surface strain energy.

It can be seen from Figure 19 that with the increase in strain energy, the deformation degree of hull surface will increase, and the variation range of wave-making resistance of the ship will also increase. This change may mean that wave-making resistance becomes smaller or larger. However, it is certain that the larger the variation range of wave-making resistance, the more likely it is to obtain a hull form with better performance in optimization.

4. Optimization Parameter Selection Based on Surface Strain Energy

In Section 3, the strain energy of the surface is used as the evaluation index of hull surface deformation. In the process of hull form optimization, it is proposed that more abundant ships can be obtained by distributing the optimization parameters in the place where the deformation degree of the hull surface is greatest. To determine the position of the maximum hull deformation surface and determine the optimal distribution of optimization parameters, a set of optimization parameter selection methods of strain energy based on a genetic algorithm is designed in this part. Taking KCS as the research object, the optimal parameter distribution is determined.

4.1. Optimization Parameter Selection Problem Definition

Firstly, a certain number of points should be selected in the discrete point cloud of the hull surface, and one- or two-dimensional coordinates of the selected points should be determined as the optimization parameters. The combination of optimization parameters with different numbers and positions will produce different deformation effects. It is a typical combinatorial optimization problem of how to maximize the deformation of the hull surface through reasonable selection of optimization parameters so as to obtain the richest ship shape possible. The mathematical description of this problem is as follows:

Discrete point cloud for n hull surfaces x_i (i = 1, 2, . . ., n), and select m points x_j (j = 1, 2, . . ., m), and a one-dimensional coordinate in x_j is determined as the optimization parameter p_j (j = 1, 2, . . ., m) (or a two-dimensional coordinate is determined as the optimization parameter p_j (j = 1, 2, . . ., m, m + 1)), the variation of each optimization parameter makes the deformation degree of the hull surface different, and the value of these m optimization parameters is required to maximize the strain energy E(p_j) of the hull surface when the surface is deformed.

Through the analysis of this problem, a mathematical model of the following form can be constructed:

$$\begin{array}{ll} \max & E\left(p_j\right) \\ s.t. & x_j \in \mathbf{X}^m \\ & \mathbf{X}^m \subset \mathbf{X}^n \end{array} \tag{17}$$

where, x_j is the selected m points, E(p_j) is the strain energy of the surface after the change of m optimization parameters, which can be solved by Equation (14), X^m is the set of selected m points, and X^n is the set of all discrete type value points.

In this example, the hull surface is composed of four NURBS surfaces, each is discretized into a point cloud of 81 × 80. If the enumeration method is used, the time cost is unacceptable. Therefore, a genetic algorithm is adopted in this example.

4.2. Optimization Parameter Selection Process

A genetic algorithm is used to solve the combinatorial optimization problem proposed in Section 4.1, and the solving process is shown in Figure 20.

Step 1: each surface of the KCS is dispersed into a point cloud of 81 × 80, and the discrete point is numbered with integers ranging from 1 to 6480.

Step 2: generate initial populations (encode chromosomes using Gray coding).

Step 3: Calculate the fitness value. The calculation method is as follows: First, the variation range of optimization parameters is determined, 100 samples are generated by uniform experimental design, and the strain energy of the hull surface of each sample after deformation is calculated. The maximum strain energy of the surface among the 100 samples is taken as the fitness value of the individual.

Step 4: Determine whether the iteration is terminated, that is, the fitness value of the individual does not change after reaching the set number of iterations or for 10 consecutive generations. If the iteration termination condition is not met, the selection (Elitist Preservation and Rank Selection), crossover (multi-point crossover), and mutation operations (bit variation operation) are carried out to generate new population individuals. Otherwise, the individual corresponding to the best fitness value is output, and the optimization ends.

In this paper, the maximum number of iterations is used as the criterion of optimization termination.

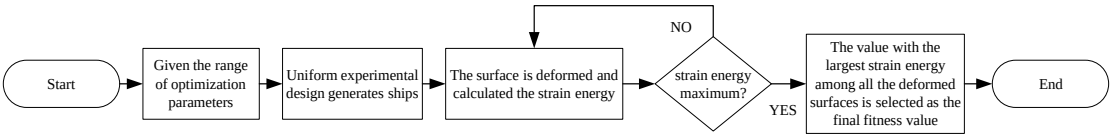


Figure 20. Flowchart of selecting optimization parameters by genetic algorithm.

4.3. KCS Optimization Parameter Selection

When choosing the optimization parameters for the bulbous bow, the bow side, and the stern of the ship, the number of optimization parameters is five, and the range of variation for each optimization parameter is ±5%. Considering the calculation amount, the iteration parameters of the genetic algorithm set in this example are presented in Table 12.

Table 12. Settings of the genetic algorithm iteration parameters in the example.

Generation	Population	Crossover Probability	Variation Probability	Inversion Probability
25	30	0.8	0.1	0.2

After optimization, the values of optimization parameters in each region are obtained, as shown in Table 13. The distribution position of optimization parameters in each region is shown in Figure 21.

Table 13. Optimization points and optimization parameters selected in each region.

Area	Optimization Point	X	Y (Optimization Parameters)	Z
Bulbous bow	P_1	0.226661	0.063854	0.122788
	P_2	0.199546	0.033786	0.060171
	P_3	0.145880	0.033610	0.269900
	P_4	0.085240	0.063548	0.230776
	P_5	0.042269	0.036654	0.129091
Bow side	P_6	0.680323	0.077100	0.267836
	P_7	1.372175	0.258909	0.271575
	P_8	2.593236	0.477493	0.212842
	P_9	2.945661	0.46849	0.115365
	P_{10}	3.210267	0.45379	0.054673
Stern	P_{11}	5.770249	0.314089	0.07463
	P_{12}	5.944755	0.403705	0.175675
	P_{13}	6.292941	0.382575	0.227046
	P_{14}	6.726653	0.265778	0.258742
	P_{15}	6.986132	0.475444	0.358739

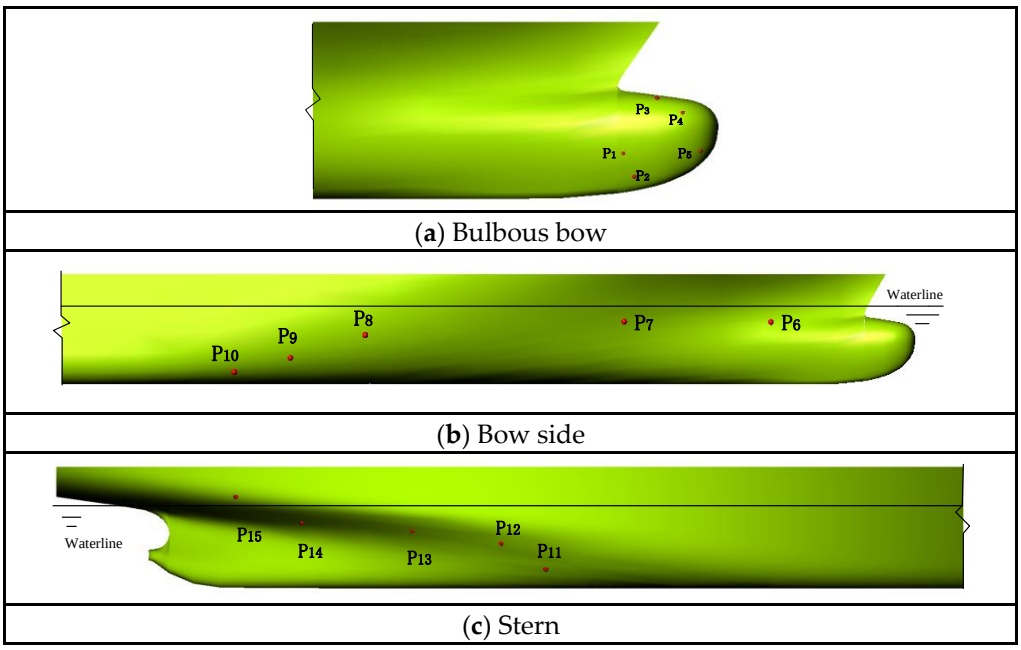


Figure 21. Optimization parameter distribution.

Intuitively, in the bulbous bow area, the optimization parameters are roughly distributed around the surface along the bulbous bow profile, which is easy to understand. When the optimization parameter distribution is relatively scattered, the greater the deformation degree of the surface and the greater the corresponding strain energy of the surface. In the bow side area, optimization parameters are mainly distributed near the flat edge line and the waterline. The flat edge line is the place where the hull surface narrows from the maximum width, where the curvature of the surface changes the most, and where the surface deformation is also the most drastic. In the stern area, the optimization parameters are also distributed in the area where the hull surface shrinks from the maximum width and near the waterline.

From the perspective of hull form optimization, when the optimization parameters are distributed near the flat side line and the waterline, the shape change of the hull surface can be more complicated, and the wave resistance of the hull can be dramatically changed.

5. Application in Hull Form Optimization

This section carries out KCS hull form optimization.

5.1. Optimization Problem Description

5.1.1. Optimization Objectives

In this example, the minimum wave-making resistance coefficient at the design speed (Fr = 0.26) is taken as the optimization objective, and the mathematical model of the optimization problem is as follows:

$$\min f_{obj} = C_w \quad F_r = 0.26 \tag{18}$$

5.1.2. Optimizing Parameter Selection

Optimization parameters need to be determined before optimization. The selection method of optimization parameters in the process of KCS optimization is as follows:

1. **Select optimization parameters based on design experience**

According to the design experience, the shape of the bulbous bow will have a great impact on the wave-making resistance optimization of the ship, among which the most

influential factors are as follows: (1) the length of the bulbous bow, (2) the width of the bulbous bow, and (3) the bulbous bow upturn/sag. In hull form optimization, the length of the bulbous bow is usually controlled by the x-coordinate value of the most front point of the bulbous bow, the upturn/sag value of the most front point of the bulbous bow is controlled by the Z-coordinate value of the most front point of the bulbous bow, and the width of the bulbous bow is controlled by the point near the maximum half width of the bulbous bow.

In this section, the point $\mathbf{P}_1$ at the most front and the point $\mathbf{P}_2$ at the most half width of the bulbous bow are selected as optimization points. The distribution of optimization points is shown in Figure 22. The X coordinate and Z coordinate of the optimization point $\mathbf{P}_1$ are taken as optimization parameters, and the Y coordinate of P_2 is taken as an optimization parameter. The optimization points and parameters selected based on design experience are shown in Table 14.



Figure 22. Distribution of optimization points selected based on design experience.

Table 14. Optimization points and parameters selected based on design experience.

Optimization Point	Optimization Parameter
$\mathbf{P}_1$	$x_1 \backslash z_1$
$\mathbf{P}_2$	y_2

2. **Select optimization parameters based on surface strain energy**

The Y coordinate of point $\mathbf{P}_3$~$\mathbf{P}_{17}$ is determined in Section 4.3 as the optimization parameter to control the deformation of the hull surface along the ship width direction.

To sum up, a total of 18 optimization parameters are determined. In addition to the optimization parameters x_1, other optimization parameters are internally changed within ±5%. The selected optimization parameters and their variation range are shown in Table 15. Optimization point distribution is shown in Figure 23.

Table 15. Optimization parameters and range.

Optimization Point	Optimization Parameter	Initial Value	Upper Bound	Lower Bound
$\mathbf{P}_1$	x_1	−0.000209	−0.1	0.0002
	z_1	0.195157	0.18539915	0.20491485
$\mathbf{P}_2$	y_2	0.074187	0.07047765	0.07789635
$\mathbf{P}_3$	y_3	0.036654	0.0348213	0.0384867
$\mathbf{P}_4$	y_4	0.063548	0.0603706	0.0667254
$\mathbf{P}_5$	y_5	0.033610	0.0319295	0.0352905
$\mathbf{P}_6$	y_6	0.033786	0.0320967	0.0354753
$\mathbf{P}_7$	y_7	0.063854	0.0606613	0.0670467
$\mathbf{P}_8$	y_8	0.07715	0.0732925	0.0810075
$\mathbf{P}_9$	y_9	0.258909	0.24596355	0.27185445
$\mathbf{P}_{10}$	y_{10}	0.477493	0.45361835	0.50136765

Table 15. *Cont.*

Optimization Point	Optimization Parameter	Initial Value	Upper Bound	Lower Bound
$\mathbf{P}_{11}$	y_{11}	0.468491	0.44506645	0.49191555
$\mathbf{P}_{12}$	y_{12}	0.45379	0.4311005	0.4764795
$\mathbf{P}_{13}$	y_{13}	0.314089	0.29838455	0.32979345
$\mathbf{P}_{14}$	y_{14}	0.403705	0.38351975	0.42389025
$\mathbf{P}_{15}$	y_{15}	0.382575	0.36344625	0.40170375
$\mathbf{P}_{16}$	y_{16}	0.265778	0.2524891	0.2790669
$\mathbf{P}_{17}$	y_{17}	0.475444	0.4516718	0.4992162



Figure 23. Optimization point distribution of KCS.

5.1.3. Constraints

1. **Fixed-point constraint**

In addition to determining the optimization parameters, it is necessary to determine the fixed point in the optimization to restrain the deformation of the hull surface. In this example, the fixed-point distribution of the deck boundary line, bottom longitudinal line, stem post, stern, and parallel body of ship are shown in Figure 24.

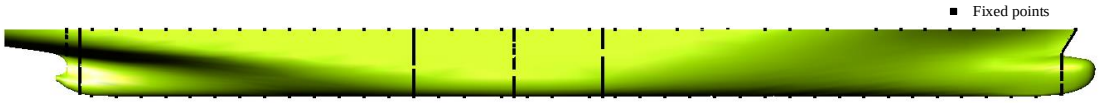


Figure 24. Distribution of fixed points.

2. **Constraints on hydrostatic parameters**

The constraint conditions of hydrostatic parameters are the same in Section 2.1.

5.2. Optimization Results

The optimization algorithm adopts a particle swarm optimization (PSO) algorithm, the iteration is 40, the particle size is 60, the weight factor is 0.8, and the learning factor is 2. The optimization iterative convergence process is shown in Figure 25, and the optimization solutions of each optimization parameter are obtained, as shown in Table 16.

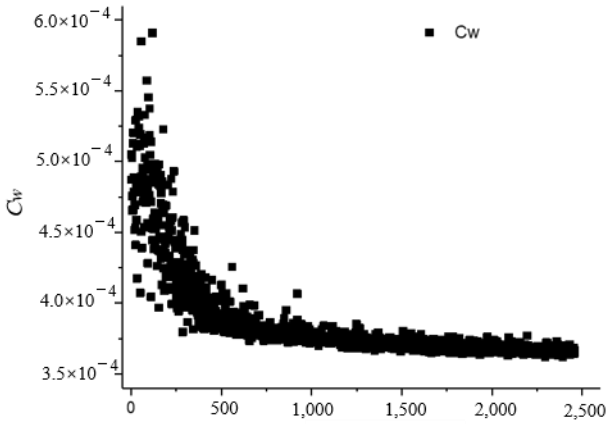


Figure 25. Optimization iterative convergence.

Table 16. Optimization solutions of each optimization parameter.

Optimization Parameter	Initial Value	Optimization Solution
x_1	−0.000209	−0.03502
z_1	0.195157	0.2049
y_2	0.074187	0.074854
y_3	0.036654	0.036064
y_4	0.063548	0.062726
y_5	0.033610	0.033906
y_6	0.033786	0.033166
y_7	0.063854	0.06248
y_8	0.07715	0.078598
y_9	0.258909	0.249659
y_{10}	0.477493	0.471858
y_{11}	0.468491	0.464632
y_{12}	0.45379	0.45281
y_{13}	0.314089	0.32195
y_{14}	0.403705	0.39769
y_{15}	0.382575	0.401704
y_{16}	0.265778	0.27906
y_{17}	0.475444	0.460652

The comparison of hydrostatic parameters and wave-making resistance between the initial ship and the optimized ship are shown in Table 17.

Table 17. Comparison of hydrostatic parameters resistance.

	Wetted Surface Area	∇	Lcb	Decrease in Wave-Making Resistance
Initial ship	9.542 m^2	1.648 m^3	3.969 m	-
Optimized ship	9.520 m^2	1.649 m^3	3.986 m	20.28%

Analysis of Table 17 reveals that compared with the initial ship, the wet surface area of the optimized ship is reduced by about 0.23%, but the ∇ is increased by about 0.06%, which is due to the fact that the bow of the optimized ship type becomes leaner while the bulbous bow becomes larger. After optimization, the wave-making resistance is reduced by about 20.28%, which achieves a relatively obvious optimization effect.

The comparison of the cross-section of the initial ship and the optimized ship is shown in Figure 22, and the comparison of the longitudinal profile is shown in Figure 23.

In the analysis of Figures 26 and 27, compared with the initial ship, the bulbous bow of the optimized ship extends forward and slightly upwarps, while the area before the parallel midbody becomes thin as a whole, making the ship shape show a thin front-end shape and changing the length of the inlet section to a certain extent. The wave rising in the bulbous bow and the wave rising in the stern are superimposed on each other to produce a favorable wave disturbance, thus reducing the wave resistance.

The waveform comparison between the initial ship and the optimized ship is shown in Figure 28, and the longitudinal wave height comparison is shown in Figure 29.

Comparing the waveforms of the initial ship and the optimized ship, it is found that the wave of the optimized ship is obviously reduced. As can be seen from the wave height diagram, between 0.5 and 2 times of length, the wave height of the optimized ship is significantly reduced, and the work of the hull to overcome the wave resistance is reduced, which is conducive to reducing the wave resistance of the ship.

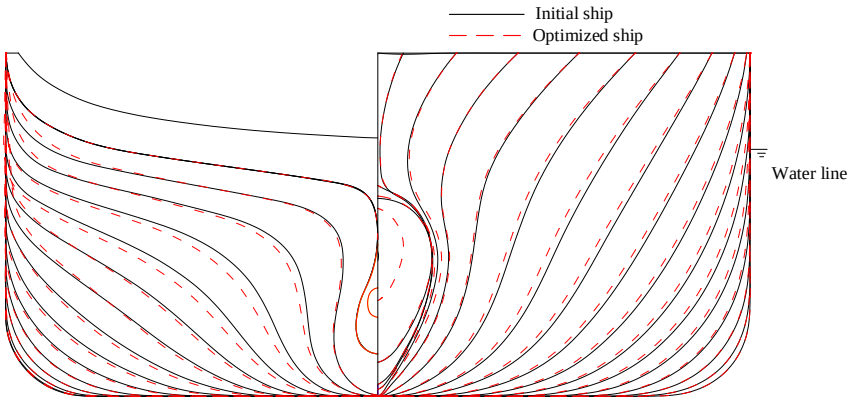


Figure 26. Cross-section comparison.

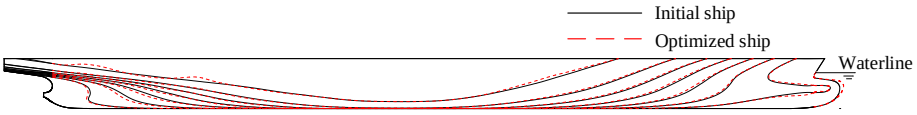


Figure 27. Longitudinal profile comparison.

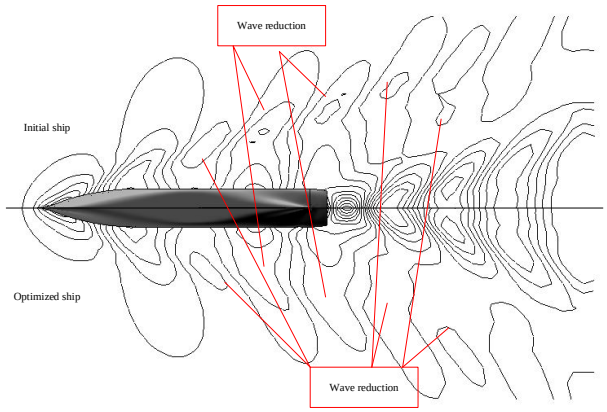


Figure 28. Waveform comparison.

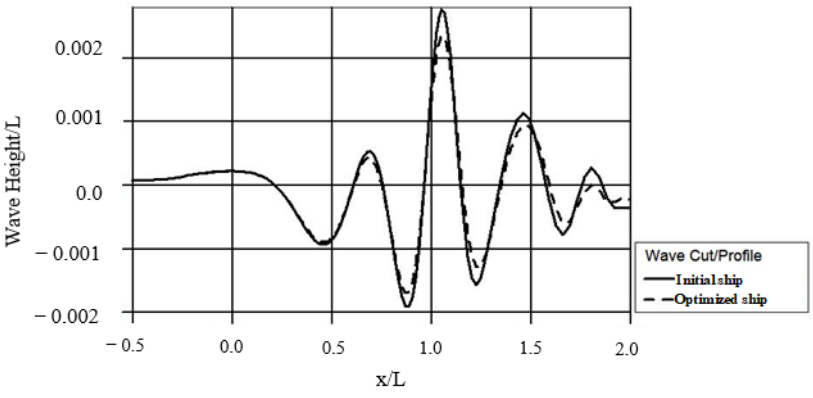


Figure 29. Longitudinal wave height comparison.

Further, the total resistance of the initial ship and the optimized ship at Fr = 0.26 was calculated. The fine grid was used for calculation, with the grid size of about 1.21 million. After 3000 iterations of calculation, the total resistance coefficient and total resistance changes of the initial ship and optimized ship are shown in Table 18.

Table 18. Comparison of total resistance.

	Total Resistance	Decrease
Initial ship	0.003555	-
Optimized ship	0.003456	−3.01%

A comprehensive analysis of KCS optimization results shows that the ship form design scheme with better resistance performance can be obtained by selecting optimization parameters according to the optimization parameter selection method proposed in this paper.

6. Summarize

Hull form optimization is a crucial technique for developing energy-efficient ships. While CFD advances have broadened its application, the rational selection of optimization parameters remains a significant challenge, often addressed subjectively based on experience. This paper proposed a systematic parameter selection method using the KCS container ship as a case study. Applying this method can enhance optimization efficiency and accelerate energy-saving hull development.

The main contributions are:

1. **Investigated the influence of parameter number and distribution:** Demonstrated that increasing the number of parameters can improve optimization quality within acceptable computational time. Found that parameter distribution in the bulbous bow area has the greatest impact on wave-making resistance optimization, followed by the bow side and stern areas.
2. **Proposed a parameter selection method based on surface strain energy:** Introduced surface strain energy as a metric for deformation degree. Established that distributing parameters to maximize hull surface deformation expands the wave-making resistance variation range, increasing the likelihood of finding superior designs. Formulated the selection as a combinatorial optimization problem solved with a genetic algorithm, determining effective parameter distributions for container ships.

The application of this method to KCS optimization achieved a 20.28% reduction in wave-making resistance and a 3.01% reduction in total resistance.

Limitations and Future Work: This study did not deeply investigate the influence of the parameter variation range, which was still determined empirically. Research into optimally setting parameter variation ranges is needed. Furthermore, while the method shows promise for container ships, its generalizability to other ship types warrants further investigation.

Despite these areas for future exploration, this paper provides a valuable, less subjective methodology for selecting optimization parameters in hull form optimization, potentially improving optimization efficiency and shortening the development cycle for energy-saving ship forms.

Author Contributions: Conceptualization, B.F.; methodology, B.F.; software, Q.Z.; validation, B.F. and Q.Z.; formal analysis, Z.L.; investigation, B.F.; resources, B.F.; data curation, Q.Z.; writing—original draft preparation, Q.Z.; writing—review and editing, Z.L., C.Z. and X.C.; visualization, Q.Z.; supervision, B.F.; project administration, Z.L.; funding acquisition, Q.Z., B.F., Z.L., C.Z. and X.C. All authors have read and agreed to the published version of the manuscript.

Funding: This research was funded by the National Natural Science Foundation of China [grant Numbers 52401390, 51979211, 52271327, 52271330, 52471339]. This study was supported by "the Fundamental Research Funds for the Cornell University (WUT:104972026RSCbs0038).

Data Availability Statement: The original contributions presented in this study are included in the article. Further inquiries can be directed to the corresponding author.

Conflicts of Interest: The authors declare no conflict of interest.

References

1. Zhao, F.; Li, S.Z.; Yang, L.; Liu, H. An overview on the design optimization of ship hull based on CFD techniques. *J. Ship Mech.* **2010**, *14*, 812–821.
2. Kim, H.J.; Choi, J.E.; Chun, H.H. Hull-form optimization using parametric modification functions and particle swarm optimization. *J. Mar. Sci. Technol.* **2016**, *21*, 129–144.
3. Campana, E.F.; Diez, M.; Liuzzi, G.; Lucidi, S.; Pellegrini, R.; Piccialli, V.; Rinaldi, F.; Serani, A. A multi-objective DIRECT algorithm for ship hull optimization. *Comput. Optim. Appl.* **2018**, *71*, 53–72.
4. Jung, Y.W.; Kim, Y. Hull form optimization in the conceptual design stage considering operational efficiency in waves. *Proc. Inst. Mech. Eng. Part M J. Eng. Marit. Environ.* **2019**, *233*, 745–759.
5. Kim, B.S.; Oh, M.J.; Lee, J.H.; Kim, Y.H.; Roh, M.I. Study on hull optimization process considering operational efficiency in waves. *Processes* **2021**, *9*, 898. [CrossRef]
6. Zakerdoost, H.; Ghassemi, H. Hydrodynamic optimization of ship's hull-propeller system under multiple operating conditions using MOEA/D. *J. Mar. Sci. Technol.* **2021**, *26*, 419–431.
7. Nazemian, A.; Ghadimi, P. Global optimization of trimaran hull form to get minimum resistance by slender body method. *J. Braz. Soc. Mech. Sci. Eng.* **2021**, *43*, 67. [CrossRef]
8. Heo, J.; Park, D.; Berg-Jensen, J.H.; Pan, Z.; Vada, T.K. Hull Form Optimization to Fulfil Minimum Propulsion Power by Using Frequency and Time Domain Potential Flow Solvers. In *Practical Design of Ships and Other Floating Structures: Proceedings of the 14th International Symposium, PRADS 2019, Yokohama, Japan, 22–26 September 2019, Volume III 14*; Springer: Singapore, 2021; pp. 220–236.
9. Grigoropoulos, G.J.; Bakirtzoglou, C.; Papadakis, G.; Ntouras, D. Mixed-fidelity design optimization of hull form using CFD and potential flow solvers. *J. Mar. Sci. Eng.* **2021**, *9*, 1234. [CrossRef]
10. Park, S.W.; Kim, S.H.; Kim, Y.I.; Lee, I. Hull Form Optimization Study Based on Multiple Parametric Modification Curves and Free Surface Reynolds-Averaged Navier–Stokes (RANS) Solver. *Appl. Sci.* **2022**, *12*, 2428. [CrossRef]
11. Renaud, P.; Sacher, M.; Scolan, Y.M. Multi-objective hull form optimization of a SWATH configuration using surrogate models. *Ocean Eng.* **2022**, *256*, 111209. [CrossRef]
12. Samuel, S.; Wicaksono, A.; Kurniawan, W.A.; Hadi, E.S.; Tuswan, T.; Trimulyono, A.; Muryadin, M. Investigation of An Inverted Bow on Frigate Hull Resistance. *J. Appl. Fluid Mech.* **2023**, *17*, 136–147.
13. Liu, J.; Zhang, B.; Lai, Y.; Fang, L. Hull form optimization research based on multi-precision back-propagation neural network approximation model. *Int. J. Numer. Methods Fluids* **2024**, *96*, 1445–1460. [CrossRef]
14. Serani, A.; Stern, F.; Campana, E.F.; Diez, M. Hull-form stochastic optimization via computational-cost reduction methods. *Eng. Comput.* **2022**, *38*, S2245–S2269.
15. Kim, W.J.; Van, S.H.; Kim, D.H. Measurement of flows around modern commercial ship models. *Exp. Fluids* **2001**, *31*, 567–578. [CrossRef]
16. Wang, P.; Feng, Y.; Chen, Z.; Dai, Y. Study of a hull form optimization system based on a Gaussian process regression algorithm and an adaptive sampling strategy, Part II: Multi-objective optimization. *Ocean Eng.* **2023**, *286*, 115501. [CrossRef]
17. Liu, Z.; Zhao, W.; Wan, D. Resistance and wake distortion optimization of JBC considering ship-propeller interaction. *Ocean Eng.* **2022**, *244*, 110376. [CrossRef]
18. Feng, B.; Yue, C.; Zhan, C.; Chang, H. Hull form multi-objective optimization of DTMB5415 ship considering arrangement constraints. In Proceedings of the Thirty-Second International Ocean and Polar Engineering Conference, Shanghai, China, 5–10 June 2022.
19. Zheng, Q.; Chang, H.C.; Liu, Z.Y.; Feng, B.W.; Jian, W.; Wei, X. Design knowledge extraction framework and its application in multi-objective ship optimization. *Ocean Eng.* **2023**, *280*, 114782. [CrossRef]

Disclaimer/Publisher's Note: The statements, opinions and data contained in all publications are solely those of the individual author(s) and contributor(s) and not of MDPI and/or the editor(s). MDPI and/or the editor(s) disclaim responsibility for any injury to people or property resulting from any ideas, methods, instructions or products referred to in the content.